MORPHOLOGY OF FUNCTIONALIZED PET-BASED ACTIVATED CARBONS

Krisztina László,[a] Katalin Marthi,[b] Francoise Ehrburger-Dolle,[c] Erik Geissler[c]
[a] *Department of Physical Chemistry, Budapest University of Technology and Economics, H-1521 Budapest*
[b] *Research Group for Technical Analytical Chemistry, Hungarian Academy of Sciences, Department of General and Analytical Chemistry, Budapest University of Technology and Economics, H-1521 Budapest*
[c] *Laboratoire de Spectrométrie Physique UMR 5588 CNRS-Université J. Fourier de Grenoble, BP 87, 38402 St Martin d'Hères cedex, France*

INTRODUCTION

Activated carbons are employed in a wide range of applications that are crucial for environmental, public health, and military security considerations. Although they are not generally perceived as high profile or even high tech materials, it is difficult to overstate their importance in modern organized society. The performance of these materials is heavily influenced not only by the available surface area and the porosity but also by the surface chemistry. Since the introduction of heteroatoms can significantly influence both their adsorption properties and their catalytic activity, it is of importance to investigate their effect. In this study, low temperature nitrogen adsorption, small angle X-ray scattering (SAXS) and scanning electron microscopy (SEM) are applied to detect the effects of surface functionalization, based on treatment with nitric acid, on the morphology of activated carbon derived from poly(ethyleneterephthalate) (PET).

EXPERIMENTAL SECTION

Granular activated carbon (APET) was prepared from PET pellets as described in ref. [1]. The surface chemistry and morphology of the precursors have been reported elsewhere[2,3]. This steam-activated carbon, obtained at 900 °C, was treated for 3 hours with concentrated nitric acid at room temperature (RT) (sample APETA) and at the boiling point (BP) of the carbon – acid suspension (sample APETB) to achieve different degrees of surface functionalization. These samples were then washed in distilled water and extracted in a Soxhlet apparatus until neutral pH was obtained. A third sample (APETW), not exposed to acid but only washed in water, was also studied as a control. The surface composition of the samples, determined by X-ray photoelectron spectroscopy (XPS), is shown in Table 1. All measurements reported here were made on samples ground in a ball mill.

Nitrogen adsorption/desorption isotherms were measured at 77 K with a Quantachrome Autosorb-1 computer controlled apparatus. The apparent surface area was derived according to the BET model. For the pore analysis the Quantachrome software was used together with the Dubinin-Radushkevich (DR) and Horváth-Kawazoe (HK) methods. The true density of the carbon samples was determined by helium pycnometry using the same instrument.

TABLE 1 Surface composition determined by XPS

sample	C atomic %	O atomic %	100 O/C
APETW	94	6	6.4
APETA	91	9	9.9
APETB	79	21	26.6

In the SAXS measurements, to take account of the wide range of characteristic sizes in these samples, a broad span of transfer wave vectors q was explored, using a synchrotron source. Ultra-small angle measurements (USAXS) were made with incident energy 7.9 keV at a sample-detector distance 216 cm. This configuration yielded measurements between ca. 7×10^{-4} and 10^{-2} Å^{-1}. A second configuration operating at 18 keV, provided data in the range 4×10^{-3} Å^{-1} = q = 1.4 Å^{-1}, where the sample to detector distances were 157 and 32cm. The detector was an indirect illumination CCD (Princeton Instruments) with effective pixel size 50 µm, cooled by a Peltier effect device. Intensity curves $I(q)$, obtained by azimuthal averaging, were corrected for grid distortion, dark current, sample transmission and also for background scattering. The powder samples were contained in capillary tubes of diameter 1.5 mm. Intensities were normalised with respect to a standard sample (lupolen), assuming an effective sample thickness of 1mm.

RESULTS

Scanning electron micrographs of the three samples [4] reveal micron-sized ridge-like texture on the surface of the carbon, which becomes more pronounced as the chemical treatment progresses. With the BP treatment the process culminates in the formation of filaments having a diameter of about 1 µm. It follows that carbon is not homogeneous in density on this length scale.

The low temperature nitrogen adsorption/desorption isotherms are shown in Figure 1. The Type I isotherms reveal a typically microporous structure with a narrow type H4 hysteresis loop, indicating slit-shaped porosity. Surface areas were calculated according to the BET model (S_{BET}). As the mechanism of adsorption in narrow pores is, however, by volume filling rather than surface layer formation, the Dubinin-Radushkevich (DR) approach was used to determine the micropore volume, W_0, from which the surface area S_{DR} was deduced. The latter calculation assumes that the molecules filling the pores are in contact with the pore walls. The characteristic energy, E_0, was determined from the slope of the DR plot with β=0.34. The pore width w of slit-shaped micropores is $2k/E_0$, where the value of the constant was taken to k=9 kJnm/mol.[5,6]. The average pore width w_{ads}(=$2V_{tot}/S_{BET}$), derived from the total pore volume and S_{BET} assuming slit-shaped geometry, is listed with the adsorption isotherm data in Table 2. The difference between S_{BET} and S_{DR} illustrates the differences between the assumptions of the two models and the real nature of the pore filling process.

The temperature of the nitric acid treatment affects the low temperature nitrogen adsorption properties and hence the morphology of the activated carbon. Sample APETW is highly microporous with S_{BET} and S_{DR} equal to 1156 and 1352 m^2/g, respectively.

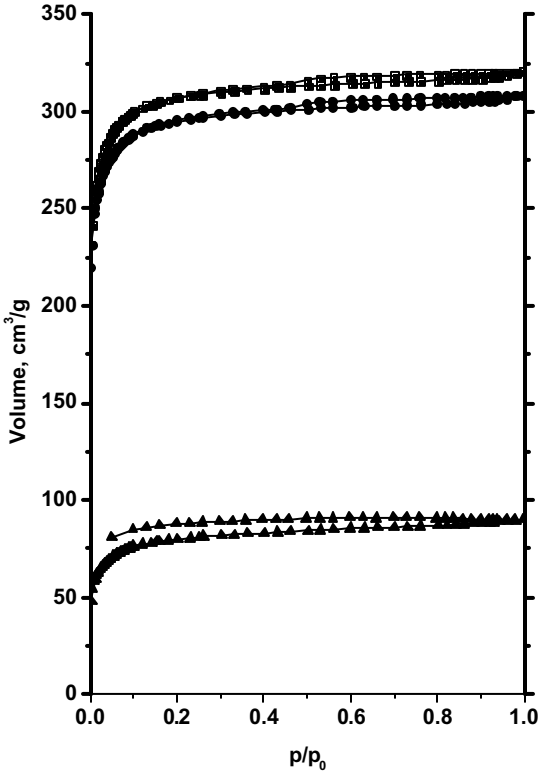

Figure 1 Low temperature nitrogen adsorption isotherms of the carbon samples. From top to bottom: APETW, APETA, APETB.

TABLE 2 Characteristic data derived from the low temperature nitrogen adsorption data

	APETW	APETA	APETB
S_{BET} m^2/g	1156	1114	304
V_{tot} cm^3/g	0.50	0.48	0.14
W_0 cm^3/g	0.48	0.46	0.12
W_0/V_{tot}	0.96	0.96	0.86
S_{DR} m^2/g	1352	1293	337
S_{BET} /S_{DR}	0.86	0.86	0.90
w_{ads} Å	8.6	8.6	9.2
w_{DR} Å	8.4	8.6	11.0

TABLE 3 Helium density and solid volume fraction ϕ

Sample	ρ_{He} g/cm^3	ϕ
APETW	1.74	0.53
APETA	1.82	0.53
APETB	1.50	0.83

RT treatment, which alters the surface chemistry [7] (Table 1), leaves the adsorption surface area of APETA practically unchanged, but slightly decreases the total porosity and the volume of the micropores (Table 2). At elevated temperature the acid treatment is more destructive (APETB). The surface area drops sharply, but the structure remains strongly microporous. The micropore volume ratio W_0/V_{tot} falls by only 10%, from 96% to 86%. These high values indicate that pore filling occurs in one step [8]. The decreased microporosity and the associated widening of the micropores slightly increases the ratio S_{BET}/S_{DR}. The damage to the pore structure is also revealed in the low pressure hysteresis (LPH). As the pore-walls have become very thin, the structure can be distorted, leading to irreversible trapping of the adsorbate molecules. Such molecules, however, escape when the evacuated sample is raised to room temperature. Entrapment takes place in pores otherwise inaccessible to the gas molecules. The low helium density of APETB (Table 3) is a sign of a severely weakened skeleton and/or selective conservation of regions with closed porosity.

The SAXS curves of the three APET samples in air are shown in Figure 2. In this figure four main regions of interest are identified, labelled (I)-(IV). In the low q region I the response of the scattering intensity $I(q)$ exhibits power-law behaviour, with a slope of about -3.6, characteristic of scattering from a fractal surface of dimension D_s=2.4.

In region II, a plateau occurs around 0.1 Å^{-1}, over which the carbon density is approximately uniform. This plateau is terminated by the shoulder at III, from which an apparent Guinier radius R_G= 6.1±0.1 Å can be deduced. If it is assumed that this scattering is caused by uniform spheres, then their outer diameter d (= 2.58R_G) is 15.8±0.3 Å. In this region, for all the samples, expressions for the single particle form factor, such as the Guinier relation or that of Debye-Bueche [9]

$$P(q) = \frac{1}{\left(1 + q^2 R_g{}^2 / 6\right)^2} \qquad (1)$$

yield a reasonable fit for the shoulder, but overestimate the intensity in the plateau region. Here R_g is the nominal radius of gyration corresponding to equation 1. The short-fall in the measured scattering intensity in the plateau region reveals spatial correlation between particles due to repulsive interactions, such as occur in dense atomic or molecular fluids [10]. Similar correlation is expected from basic structural units (BSUs) forming a disordered nanoporous carbon matrix. The total scattered intensity from the assembly of such particles may be approximated by the product of the particle form factor $P(q)$ and the structure factor $S(q)$,

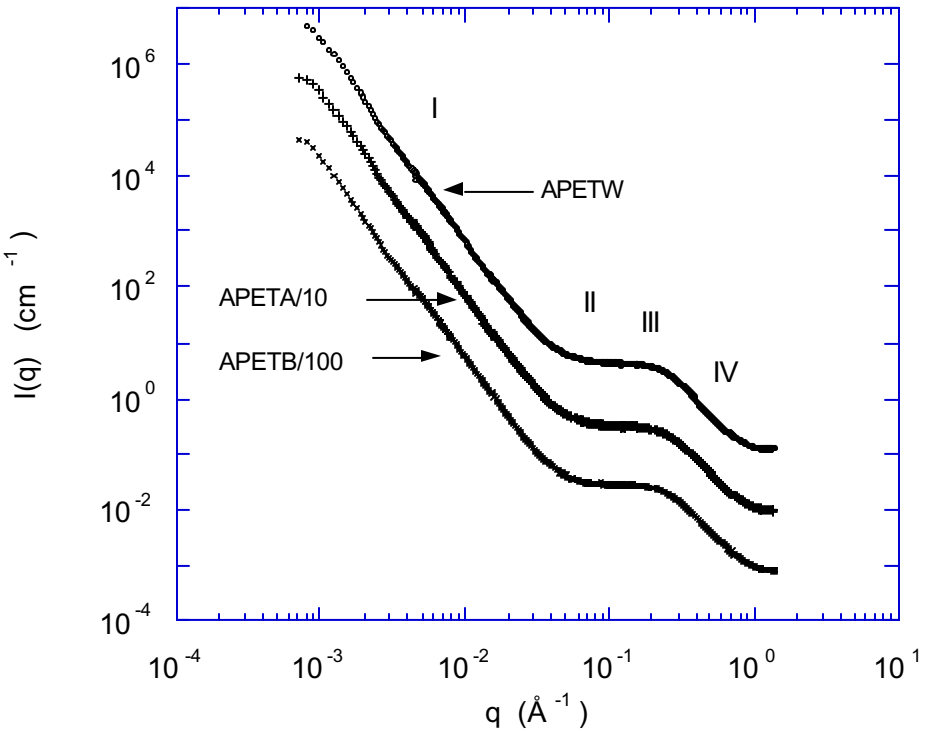

Figure 2 SAXS spectrum of the three samples APETW, APETA and APETB in air, showing the four zones described in the text. APETA and APETB have been shifted vertically downward by one and two decades, respectively.

$$I(q) = S(q)\, P(q) \tag{3}$$

where $S(q)$ describes the interference due to interparticle correlation. Figure 3 shows the structure factor $S(q)=I(q)/P(q)$ calculated for sample APETW in the shoulder region III of Figure 2, where expression (1) has been used for $P(q)$. $S(q)$ exhibits a weak maximum around $q_m \approx 0.3$ Å^{-1}, corresponding to a mean separation L between the BSUs. If the latter were arranged in crystalline order, a diffraction peak would be observed at $q_m=2\pi/L$. In disordered interacting systems, however, the peak is broadened. Expressions for $S(q)$ have been developed for hard spheres[11] an approach that has been recently employed to describe the distribution of micropores in activated carbon fibres[12]. In the present case of a frozen assembly of objects of irregular shape, however, no general analytical expression exists for $S(q)$. The following simple empirical fitting function[13], however, has been found to give reasonable agreement with computer simulations of $S(q)$[14]

$$S(q) = \frac{1}{1+3\,p(\sin qL - qL\cos qL)/(qL)^3} \tag{4}$$

where the amplitude of the correlation peak is described by the parameter p. The position of the first maximum of eq 4 at $q_mL=5.76$ indicates a separation of $L \approx 19$ Å

between the BSUs. The estimated values of L for the three samples (Table 4) decrease slightly for APETA and APETB.

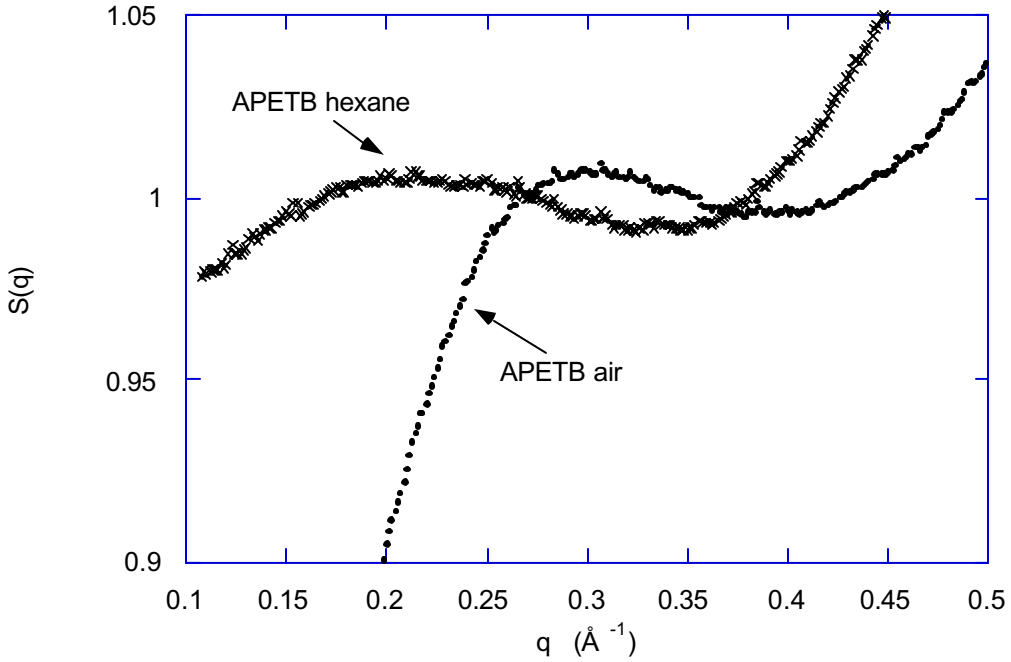

Figure 3 Structure factor $S(q) = I(q)/P(q)$ calculated for sample APETB in air (+) and in liquid hexane (x), where $P(q)$ is given by eq 1.

A correlation peak implies that the model associated with eq. 1 is not suitable for determining the specific surface area of the activated carbon for X-rays. Instead, the Porod approach is employed [15]. A region of the scattering spectrum is sought where the Porod law holds, i.e., where the intensity varies as q^{-4}. The observed slope in region IV, however, is only -2.5. Owing to atomic disorder in the surrounding material, this region at high q contains an additional signal that varies only weakly with q. In what follows, it is assumed that the background signal from atomic disorder, b, is constant and independent of q in this region. The total intensity is then

$$I(q) = Kq^{-4} + b. \tag{5}$$

Hence

$$I(q)\, q^4 = K + bq^4. \tag{6}$$

The values of the slope b are listed in Table 4. The specific surface area $S_X = A/V\rho_{av}$, where ρ_{av} is the macroscopic sample density and A/V is the area per unit volume of sample, is then found from [15]

$$\frac{A}{V} = \frac{\pi\phi(1-\phi)K}{\int_0^\infty (I(q) - b)\, q^2 dq} \tag{7}$$

The values of the volume fraction ϕ and the density ρ_{av} are determined by a combination of gas adsorption and helium pycnometry results (Tables 2 & 3). In these samples, the invariant $Q=\int_0^\infty (I(q)-b)q^2dq$ in the denominator of equation (7) is sensitive both to the upper and lower limits of the integral. A knowledge of the scattering behaviour at q=0 and q=∞ is therefore essential, since the whole of the scattering curve must be included. The contribution from the upper limit is, from equation 4

TABLE 4 Parameters derived from SAXS

Sample		R_G Å	L Å	b (cm^{-1})	S_X m^2/g	S_{BET}/S_X (S_{DR}/S_X)	$w_{min}=2V_{tot}/S_X$ (Å)
APETW	air	6.1	19.6	0.099	2000	0.58 (0.68)	5.0
	hexane	5.4	19.6	0.045	1980	0.58 (0.68)	5.1
APETA	air	5.8	19.1	0.082	1970	0.56 (0.58)	4.9
	hexane	5.6	19.8	0.045	2050	0.54 (0.63)	4.7
APETB	air	5.8	18.9	0.078	860	0.35 (0.39)	3.3
	hexane	6.0	27.2	0.056	520	0.58 (0.65)	5.4

$$\int_{q_{max}}^{\infty} (I(q)-b)q^2dq = \int_{q_{max}}^{\infty} \frac{K}{q^2}dq = K/q_{max} \qquad (8)$$

where q_{max} is the highest value of q explored in the fit to eq 5. For q_{max}=1.0 $Å^{-1}$, this contribution amounted generally to about 20% of the total value of the invariant.

The lower limit of the integral in Q is determined from the electron micrograph images [4], which indicate typical sizes close to 1 μm, i.e., a lower limit of $q_{min}=10^{-4}$ $Å^{-1}$. The resulting contribution to Q from the region $q_{min}=q$=0.01 $Å^{-1}$ was found to amount to 15-25% of the total. These results thus suggest that estimates of the specific surface area of activated carbons can be substantially in error unless both upper and lower q ranges of the SAXS spectra are taken into account.

The values found for S_X are listed in Table 4. They are smaller than the notional limiting value of the graphene unit (ca. 2600 m^2/g) but still larger than the surface areas derived from adsorption data (S_{BET} and S_{DR}), as indicated by the ratio S_{BET}/S_X or S_{DR}/S_X. The possible contribution from inaccessible pores can be directly verified by contrast variation. This technique consists in bathing the carbon in a low molecular weight fluid, which reduces the signal from regions in the sample that are penetrated by the liquid, while leaving unaffected the intensity scattered by regions from which the liquid is excluded. Figure 4 shows, as a typical example, three SAXS responses of the same sample (APETA), in the dry state, with hexane vapor (partial pressure $p/p_0\approx0.4$), and

also in contact with liquid hexane. At low q the response of the hexane vapor sample is identical to that of the dry specimen, i.e., the space between the surfaces of the large structures is filled with hexane vapor. At higher q the hexane vapor curve deviates to join that of the sample containing liquid hexane. The hexane fills the micropores in the condensed state, thereby reducing the electron density contrast in that region of the spectrum. At the upper end of the explored range of q ($\approx$1.25 Å^{-1}), the carbon-air and carbon-hexane curves meet again, demonstrating that the hexane molecules are totally excluded from this part of the spectrum. This value of q corresponds to an exclusion size limit $d_{min} \approx 2\pi/q$=5Å.

The carbon-liquid hexane curves can be analysed using eqs 6-7, in the same way as for the carbon-air samples, to calculate the surface area S_{Xhex} of carbon in contact with the hexane (Table 4). It is notable that the values of the constant b in equation 5 are smaller than for the carbon-air specimens. This observation indicates that the structure contributing to atomic disorder is partly penetrated by the hexane molecules, i.e., the walls of the pores are not smooth but contain cavities in which the hexane molecules nest, an effect called *captation* [16]. Those parts of the carbon matrix into which the

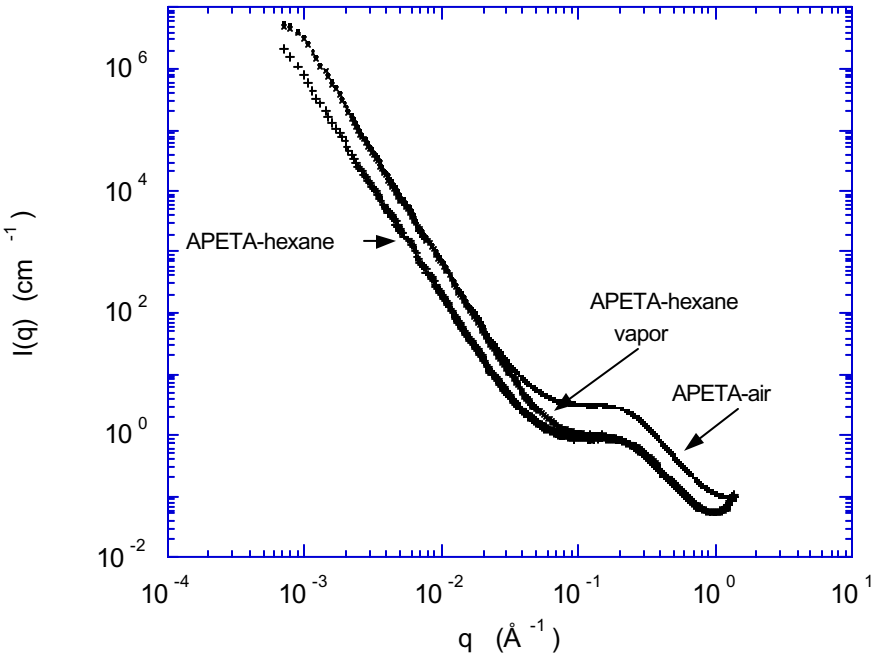

Figure 4 SAXS spectra of sample APETA in air, in hexane vapor and in liquid hexane. The APETA-hexane vapor curve is identical to that of the APETA-air sample at low q, but at $q \geq 0.1$ A^{-1}, it joins that of the liquid hexane. This shows that hexane in the micropores is in liquid state.

hexane molecules cannot nest have a higher contrast and the signal at high q accordingly increases. The striking result of these measurements, shown in Table 4, is that in samples APETW and APETA, S_X is equal to S_{Xhex} within experimental error. It follows immediately that in these samples the difference between any of the adsorption derived surfaces and S_X cannot be attributed to permanently closed pores.

For APETB, on the other hand, S_{Xhex} is intermediate between S_X and the adsorption surface listed in Table 2, but each of the ratios S_{BET}/S_{Xhex} or S_{DR}/S_{Xhex} adopts the same

value as in the other two samples. Here it may be reasonable to attribute the differences, at least in part, to inaccessible pores. Indeed, their presence is likely, in view both of the LPH in the adsorption curve of this sample (Figure 1) and of the low value of ρ_{He}. These observations confirm the deformable structure of this sample. The presence of hexane molecules in one pore can close neighbouring pores in a random way, a phenomenon that also can happen during nitrogen adsorption. Direct evidence for such local mechanical deformation is found in the change of the structure factor S(q) when hexane is added (Figure 3). The resulting value of *L*, the inter-BSU distance, increases from about 19 Å in the dry sample to 27 Å in the presence of hexane (Table 4). Such local swelling is consistent with the existence of LPH. In samples W and A, however, the corresponding variation of L is small and similar to the experimental error.

An independent measure of the minimum characteristic distance in the sample, w_{min}, is determined by the ratio V_{tot}/S_{Xhex}, assuming that the Gurvitsch rule holds. This is often the case when the adsorption isotherm is of Type I. Deviation from the Gurvitsch rule may arise when a molecular sieve effect occurs. The pore then has a width of less than two molecular diameters[17]. For slit geometry, the width w_{min} is equal to $2V_{tot}/S_{Xhex}$. From the data given in Table 4, this yields the values w_{min}=5.1, 4.7 and 5.4 Å in samples APETW, APETA and APETB, respectively. These results are larger than the calculated critical molecular size of hexane 4.0Å[18]. Empirical limiting sizes, indicating the smallest slit size into which a hexane molecule can be fitted, range between 4.3 and 4.9Å[17,19]. The evidence thus tends to show that there is a single layer of hexane between the slit walls. On the other hand, the slit widths derived entirely from adsorption data (listed in Table 2) range from 8.4 to 11.0 Å.

In view of the differences in surface chemistry and adsorption properties, the similarity of the SAXS spectra from the carbon-air samples, which is illustrated by the similarity of all the parameters deduced purely from SAXS, may seem surprising. Differences among these samples in their X-ray specific surface area stem essentially from the differences in density and in pore volume, which are determined by an independent technique. The nanoporous regions, which are preferentially destroyed in the BP acid reaction, have a higher true density than other regions with small inaccessible voids.

CONCLUSION

Surface functionalization of activated carbon by exposure to nitric acid modifies the chemistry of the solid material, depending on the severity of the treatment. XPS reveals a moderate increase in the surface oxygen content, from 6 to 9 at%, and a much larger enhancement to 21 at% for acid treatment at room or elevated temperature, respectively. The significant difference in the surface chemistry influences mainly the finer structure. The carbons display an apparent surface fractal dimension of D_s=2.4 in the wave vector range 0.001Å^{-1}-0.02 Å^{-1}.

The control sample is strongly microporous with a BET and a DR surface area of 1156 and 1352 m^2/g, respectively. 96 % of its pores contribute to the 0.48 cm^3/g micropore volume. The minimum slit width available either for nitrogen or hexane is 5.1Å from the X-ray and pore volume data. It is composed of randomly packed turbostratic basic structural units with an average separation *L* of 19.6Å. The X-ray derived surface area S_X, measured both in air and in hexane is about 2000 m^2/g.

For the room temperature treated sample the adsorption derived surface areas (BET: 1114 m^2/g, DR: 1293 m^2/g) and the X-ray derived surface areas (ca. 2000 m^2/g) are

practically unchanged. The marginally smaller micropore volume (0.46 cm^3/g) amounts to the same fraction of the total porosity. The average and the minimum slit widths as well as the separation of the basic structural units are virtually unaffected.
The damage caused by the boiling acid causes a loss of about 75 % in the measured surface areas. A weakening of the pore walls is sensed by several indicators: low helium density, pronounced low pressure hysteresis and swelling of the separation between basic structural units when hexane is introduced (from 18.9 to 27.2 Å). The greater hydrophilic character also may contribute to this effect. The minimum slit width expands from 3.3 Å in air to 5.4 Å in hexane.

ACKNOWLEDGEMENTS
Access to the small angle beamline BM2 at the European Synchrotron Radiation Facility is gratefully acknowledged. Our thanks to E. Fülöp and G. Bosznai for sample preparation and to J. F. Bérar, D. Djurado, K. Kosik, F. Livet and C. Rochas for discussions and valuable assistance. This research was supported by the National Research Fund (OTKA, grant No. T 025581) and the National Research and Development Programs (NKFP 3/043/2001).

REFERENCES
[1] László, K.; Bóta, A.; Nagy, L.G.; Frischkorn, C.B. *Carbon* **1997**, *35*, 593.
[2] Bóta, A.; László, K.; Nagy, L.G.; Copitzky, T. A. *Langmuir* **1997**, *13*, 6502.
[3] László, K.; Bóta, A.; Dékány, I. *Carbon* **2003**, *41*, 1205.
[4] László, K., Marthi, K., Rochas, C., Ehrburger-Dolle, F., Livet, F., Geissler, E. *Langmuir* 2004, 20, 1321.
[5] Stoeckli F.; López-Ramón M.V.; Hugi-Cleary, D.; Guillot, A. *Carbon* **2001**, *39*, 115.
[6] Nguyen, C.; Do, D.D. *Carbon* **2001**, *39*, 1327.
[7] László, K.; Kerepesi, P.; Tombácz, E.; Josepovits, K.; Geissler, E. *Carbon'02 International Conference on Carbon*, 2002. September 15-19, Beijing, China, CD ROM of Extended Abstracts E046, 4 pp
[8] Carrot, P.J.M.; Roberts, R.A.; Sing, K.S.W. *Carbon* **1987**, *25*, 59.
[9] Debye, P.; Bueche, R.M. *J. Appl. Phys.* **1949**, *20*, 518.
[10] Enderby, J.E.; March, N.H. *Adv. Phys* (*Phil. Mag. Suppl.*) **1965**, *14*, 453.
[11] Percus, J.K., Yevick, G.J. *Phys. Rev*. **1958**, *110*, 1.
[12] Hoinkis, E.; Ziehl, M. *Carbon* **2003**, *41*, 2047.
[13] Posselt, D.; Pederson, J.S.; Mortensen, K. *J. Non-Cryst. Solids* **1992**, *145*, 128.
[14] Hasmy, A.; Anglaret, E.; Foret, M.; Pelous, J.; Jullien, R. *Phys. Rev. B* **1994**, *50*, 6006.
[15] Porod, G. In *Small Angle X-ray Scattering;* Glatter, O., Kratky, O., Eds., Academic Press, London 1982.
[16] Pászli, I.; László, K. *Progress in Colloid and Polymer Science,* **2001**, ***117***, 51.
[17] Gregg, S.J.; Sing, K.S. *Adsorption, Surface Area and Porosity*; Academic Press: London, 1982.
[18] Breck, D.W. In *Zeolite Molecular Sieves*, Wiley, New York, 1974, p 636.
[19] Webster, C.E.; Drago, R.S.; Zerner, M.C. *J. Am. Chem. Soc*. **1998**, *120*, 5509.